

Coherent-Potential Approximation in a Two-Band Model: Electronic and Transport Properties of Semiconducting Binary Alloys*†

P. N. Sen†

Department of Physics and The James Franck Institute, The University of Chicago, Chicago, Illinois 60637

(Received 1 September 1972; revised manuscript received 16 April 1973)

The formalism of the coherent-potential approximation is extended to include the two-band case. The single-site energy of the one-band case is replaced by a 2×2 matrix which varies randomly from site to site according to the occupancy of the site. The Kubo formulas for transport are also extended for the two-band model giving a nonvanishing vertex correction as opposed to the zero vertex correction for the single-band model. The cases treated explicitly correspond to fully disordered binary semiconducting alloys. The band gap and bandwidths are chosen as representative of typical semiconductor values, and concentrations, band gaps, gap centers, and band mixing are all varied systematically. Results are reported for densities of states, parentage, dc conductivity, and the imaginary part of the dielectric constant $\epsilon_2(\omega)$. The analytic behavior of $\epsilon_2(\omega)$ near threshold corresponds to several experimental situations.

I. INTRODUCTION

Recently, much experimental and theoretical work has been done on¹⁻³ amorphous and alloy semiconductors. In the crystals the energy of excitations can be described by a dispersion relation $E(\vec{k})$, where \vec{k} is the wave vector. In the disordered materials \vec{k} ceases to be a good quantum number, and the simplicity is lost. Nevertheless, experiments indicate that many of the electronic properties of disordered materials resemble those of pure crystals.

There is a large class of alloys which exhibit well-defined electronic, optical, and transport properties which vary continuously with composition between those of the pure components like Si-Ge (elemental), $(\text{In}_x\text{Ga}_{1-x})\text{As}$, $(\text{Hg}_x\text{Cd}_{1-x})\text{Te}$, and $(\text{Pb}_x\text{Sn}_{1-x})\text{Te}$. The similarity of these alloys to the perfect crystals can presumably be explained by the fact that the difference of pseudopotentials of the components is small compared to the over-all bandwidths and they exhibit lattice periodicity.

The resemblances between amorphous and perfect crystalline semiconductors are primarily due to the fact that the short-range order is not affected greatly in going from the crystalline to the disordered form. However, band edges cease to be sharply defined, with tails of localized states forming in the band gap, and mobility edges appear. A coherent physical picture of these materials is yet to emerge. Theories, like the Mott-Cohen Fritzsche-Ovshinsky (CFO) model,⁴ are just the beginning. Nevertheless, there are certain key features of the electronic structure of disordered materials which are quite universal, and one can therefore hope to learn about these basic features by studying models of substitutional binary alloys, in which the disorder potential can be made arbitrarily large, much larger than in typical real alloys and comparable to that in amorphous solids.

Motivated by these facts, we study substitutional binary alloys both for their intrinsic interest and for a deeper understanding about amorphous semiconductors.

For simple substitutionally disordered binary alloys, the coherent-potential approximation (CPA) has been demonstrated⁵⁻⁹ to be superior, for practical quantitative calculation, to other known theoretical techniques. The effects due to lattice disorder or clustering, such as appearance of tails of localized states and the mobility edges, lie outside its scope. However, Economou *et al.*¹⁰ have generalized the CPA to obtain information about mobility edges in disordered materials. In brief, the CPA provides an excellent practical computational scheme for disordered binary alloys.¹¹⁻¹³

In this paper we generalize the CPA to include two bands with arbitrary band mixing and thereby study various electronic properties of semiconducting alloys. It is well known¹⁴⁻¹⁷ that the gross features of the optical and photoemission properties of sp^3 hybridized, tetrahedrally bonded semiconductors of zinc-blende and diamond structure can be described by a two-band model. Semiconductors are characterized by a large bandwidth and a small band gap¹⁸; the effects of band mixing in alloying are very important and are properly taken into account. Since the scattering strength and hence the degree of disorder can be made large, we can hope to mimic characteristics of amorphous and liquid semiconductors as well.

The present paper is divided into the following sections: In Sec. II A we present a general formalism for extending the CPA to include two bands. In Sec. II B we work out several limits and discuss the parentage of states and the density of states. In Sec. III, we generalize Velicky's formalism for the transport coefficients to include two bands. The transport properties are given by the average of a product of two Green's functions, a generaliza-

tion of the Kubo¹⁹ formula. Velicky^{20,21} showed that in the CPA this average can be decomposed into a product of two average Green's functions and another term which contains so-called vertex corrections. In the one-band model, the vertex correction vanishes.²⁰ The vertex correction turns out to be nonzero and important for a two-band model even in the single-site approximation. In Sec. IV A we introduce and justify a model which we use for numerical examples for binary semiconducting alloys. In Sec. IV B we present the densities of states, parentages, and band gaps for the various values of the parameters. We also point out qualitative agreement with the general experimental trends.¹⁸ In Sec. IV C we present the results of the calculations for dc conductivity and for the imaginary part of the dielectric constant $\epsilon_2(\omega)$. We conclude in Sec. V by discussing the significance of our results.

II. CPA

A. Generalization to Include Two Bands

In this section we generalize the CPA to include two bands with arbitrary band mixing. The single-electron Hamiltonian is written in tight-binding form as

$$H = \sum_n |n\rangle \begin{pmatrix} \epsilon_n^{11} & \epsilon_n^{12} \\ \epsilon_n^{21} & \epsilon_n^{22} \end{pmatrix} \langle n| + \sum_{m \neq n} |m\rangle \begin{pmatrix} t_{mn}^{11} & 0 \\ 0 & t_{mn}^{22} \end{pmatrix} \langle n| \quad (2.1)$$

or

$$H = \hat{D} + \hat{W}. \quad (2.2)$$

$|n\rangle$ is the Wannier orbital at site n . We will assume, in the spirit of the CPA, that the elements ϵ_n^{ij} ($i, j = 1, 2$) are random from site to site and that the elements t_{mn}^{ii} ($i = 1, 2$) are independent of the occupancy at sites m and n . \hat{D} denotes, again, the random part, which is diagonal in the site index but off-diagonal in the band indices, while \hat{W} denotes the periodic part, which is diagonal in the band indices but off-diagonal in the site indices. We have chosen the representation where t_{ij} is diagonal. If we restrict ourselves to real matrix elements, Hermiticity requires that

$$t_{mn}^{ii} = t_{nm}^{ii} \quad (i = 1, 2) \text{ for all } m, n, \quad (2.3)$$

$$\epsilon_n^{12} = \epsilon_n^{21} \text{ for all } n. \quad (2.4)$$

The one-electron Green's function for the alloy for a complex energy Z is given by

$$G(Z) = \frac{1}{Z - H} = \frac{1}{Z - \hat{D} - \hat{W}}. \quad (2.5)$$

Some of the averaged properties of alloys are given by the ensemble average of the Green's function $\bar{G}(Z)$ over the alloy configuration. \bar{G} is defined through a self-energy $\Sigma(Z)$, which stands for an effective potential felt by an electron of energy Z . We denote the average over alloy configuration by $\langle \dots \rangle$:

$$\bar{G}(Z) = \langle G(Z) \rangle = \frac{1}{Z - \hat{D} - \hat{W}} = \frac{1}{Z - \hat{W} - \Sigma(Z)}, \quad (2.6)$$

$$\Sigma = \sum_n |n\rangle \Sigma_n(Z) \langle n|.$$

At each site the deviation from the effective medium, $\epsilon_n - \Sigma_n(Z)$, defines a local t matrix t_n :

$$|n\rangle t_n(Z) \langle n| = |n\rangle [\epsilon_n - \Sigma_n(Z)] \times \{1 - \langle n | \bar{G}(Z) | n \rangle [\epsilon_n - \Sigma_n(Z)]\}^{-1} \langle n|. \quad (2.7)$$

The CPA equation for Σ , which is now a 2×2 matrix equation in the band indices, is given by requiring $\langle t_n \rangle = 0$:

$$\Sigma(Z) = \epsilon - [\epsilon^A - \Sigma(Z)] \bar{F}(Z) [\epsilon^B - \Sigma(Z)]. \quad (2.8)$$

Here \bar{F} is a 2×2 matrix in the band indices and is given by

$$\bar{F}(Z) = \langle n | \bar{G}(Z) | n \rangle = \frac{1}{N} \sum_{\mathbf{k}} \langle \mathbf{k} | \bar{G}(Z) | \mathbf{k} \rangle, \quad (2.9)$$

where $|\mathbf{k}\rangle$ are Bloch states and band indices are implied;

$$\epsilon = x\epsilon^A + y\epsilon^B, \quad (2.10)$$

where x and y stand for the concentration of A and B components, respectively. In Eq. (2.8) we have dropped the superfluous subscript n . The average density of states for the alloy $\rho(E)$ is given by

$$\rho(E) = - (1/\pi) \text{Im Tr} \bar{G}(E + i0) = - (1/\pi) \text{Im} [\bar{F}_{11}(E + i0) + \bar{F}_{22}(E + i0)]. \quad (2.11)$$

B. Limiting Cases of CPA, Parentage, and Moments

Let us define the Green's function for what we shall call the pure crystal by $G^0(Z)$, where $\epsilon^A = \epsilon^B = 0$, i. e., $G^0 = (Z - \hat{W})^{-1}$. Then the Dyson equation for Σ is given by

$$\bar{G} = G^0 + G^0 \Sigma \bar{G}. \quad (2.12)$$

If the dispersion relations for the energy bands in the pure crystal are given by $E_1(\mathbf{k})$ and $E_2(\mathbf{k})$ for the valence band (band 1) and conduction band (band 2), respectively,

$$E_i(\mathbf{k}) = \frac{1}{N} \sum_{m,n} e^{i\mathbf{k} \cdot (\mathbf{R}_m - \mathbf{R}_n)} t_{mn}^{ii}, \quad i = 1, 2$$

then the densities of states of the pure crystal for bands 1 and 2 are

$$\rho_{ii}^0 = \frac{1}{N} \sum_{\mathbf{R}} \delta(E - E_i(\mathbf{k})), \quad i=1, 2. \quad (2.13)$$

The total density of states in the pure crystal is given by Eq. (2.11), where ρ , \bar{G} , and \bar{F} are replaced by ρ^0 , G^0 , and F^0 . The energy spectrum of the quasiparticles will coincide with the poles of the continuation of $\bar{G}(\mathbf{k}, Z)$ in the second sheet. Such poles will be given by the solution of

$$\det | E - \epsilon(\mathbf{k}) - \Sigma(E^-) | = 0. \quad (2.14)$$

The lifetime of these quasiparticles will be related to $\text{Im}\Sigma(E)$ which has all \mathbf{k} vectors mixed in.

Moments. One can write down the moment expansion for $\bar{G}(Z, \mathbf{k})$; the explicit evaluation of these for our case is laborious and seems to give no further insight. In scalar case Velicky, Kirkpatrick, and Ehrenreich⁶ were able to demonstrate that the CPA gives more exact moments than the rigid-band or virtual-crystal approximation.

Weak-Scattering Limit $\delta \rightarrow 0$

Let us define a quantity δ by the 2×2 matrix

$$\delta = \epsilon^A - \epsilon^B.$$

It can be shown easily then from (2.8) that, as $\delta \rightarrow 0$,

$$\Sigma \rightarrow \epsilon + xy\delta F_\epsilon \delta, \quad (2.15)$$

$$F_\epsilon = \frac{1}{N} \sum_{\mathbf{k}} \left\langle k \left| \frac{1}{E - \bar{W} - \epsilon} \right| k \right\rangle.$$

Dilute Alloy Limit $x \ll 1$

One obtains

$$\Sigma \rightarrow \epsilon + (1 - \delta F_{\epsilon B})^{-1} x \delta F_{\epsilon B} \delta. \quad (2.16)$$

Split Band Limit $\delta \gg 1$

Velicky, Kirkpatrick, and Ehrenreich⁶ (VKE), by considering moments, were able to obtain the limit $\delta \gg 1$ and were able to find a necessary and sufficient condition for the appearance of a pole in Σ which corresponds to a zero of F and indicates the splitting of the band. We have obtained some analogous criteria, only for certain cases, for the model we used in numerical examples (see Sec. IV B).

Virtual Crystal Approximation (VCA)

See Appendix A for details. In this limit the Hamiltonian is replaced by an average Hamiltonian and Σ becomes equal to ϵ identically. The similarity of substitutional semiconductor alloys to those of pure crystal suggests that might be reasonable. Van Vechten *et al.*¹⁸ have shown that this is not true.

Parentage

The bounds of the spectrum of the alloy are those of the union of the spectrum of pure components

(Lifshitz²² limits). We can obtain significant insight in relation to these limits when the contribution to the total density of states originating from each component is explored. To this end we seek a decomposition into components as follows:

$$\rho(E) = x\rho^A(E) + y\rho^B(E). \quad (2.17)$$

ρ^A and ρ^B can be obtained by replacing one site, say n , by a specified atom or molecule A or B in the effective medium while the potential at the rest of the sites is given by $\Sigma(Z)$. If G^A and G^B are the corresponding Green's functions, then we have

$$F^{A,B}(Z) = \langle n | G^{A,B}(Z) | n \rangle \\ = \{1 - \bar{F}(Z)[\epsilon^{A,B} - \Sigma(Z)]\}^{-1} \bar{F}(Z). \quad (2.18)$$

Using the equation $\langle t \rangle = 0$, we see that (2.18) becomes

$$\bar{F}(Z) = xF^A(Z) + yF^B(Z). \quad (2.19)$$

Then Eq. (2.17) follows immediately from Eq. (2.19) by the use of Eq. (2.11) with $\rho^{A,B}$ defined by substituting $F^{A,B}$ for \bar{F} in (2.11).

Noting that as $x \rightarrow 0$, $\Sigma(Z) \rightarrow \epsilon^B$ and using (2.10) and (2.16), we get

$$\rho_{\epsilon A} \rightarrow - (1/\pi) \text{Im Tr} [1 - F_{\epsilon B}(\epsilon^A - \epsilon^B)]^{-1} F_{\epsilon B}(Z). \quad (2.20)$$

This is exactly the Köster-Slater^{23,24} formula for the density of states at a single impurity site occupied by an A -type atom embedded in a pure crystal made of B atoms. The density of states at an impurity site can be a δ function in the Köster-Slater problem, corresponding to a localized state. In the CPA, the δ function is smeared due to the finite imaginary part of the self-energy.

III. TRANSPORT AND INTERBAND OPTICAL PROPERTIES

Velicky²⁰ reexpressed the Kubo¹⁹ formula for the transport coefficient in terms of a product of two Green's functions and showed how to average it in the framework of the CPA. In this section we generalized Velicky's work for the two-band model. The conductivity tensor $\sigma_{\mu\nu}(\omega)$ at a frequency ω is given, in the long-wavelength limit, by the current-current (j - j) response function. After some simplification assuming cubic point symmetry ($\sigma_{\mu\nu} = \sigma_{\nu\mu}$, etc.). We can rewrite the dc conductivity σ and ϵ_2 , the imaginary part of dielectric function, in the following way: Let

$$\sigma(E) = \text{Tr}_s \langle j \delta(E - H) j \delta(E - H) \rangle; \quad (3.1)$$

then

$$\sigma(\omega = 0) = \sigma = \pi \int_{-\infty}^{\infty} -dE \frac{\partial f}{\partial E} \sigma(E), \quad (3.2)$$

$$\epsilon_2(\omega) = \frac{4\pi^2}{\omega^2} \int_{-\infty}^{\infty} dE [f(E) - f(E + \omega)] \\ \times \text{Tr}_s \langle j \delta(E - H) j \delta(E + \omega - H) \rangle,$$

and

$$\delta(E - H) = -(1/2\pi i)[G(E^+) - G(E^-)]. \quad (3.3)$$

Here f is the usual Fermi function, j the current operator, Tr_s denotes the trace over single-particle states and $\langle \dots \rangle$ denotes the average over alloy configurations. It is clear that we have to compute quantities like

$$K(Z_1, Z_2) = \langle G(Z_1) j G(Z_2) \rangle. \quad (3.4)$$

G is the full Green's function given by (2.5). Following Velicky,²⁰ one defines the vertex correction Γ as follows:

$$K(Z_1, Z_2) = \bar{G}(Z_1) j \bar{G}(Z_2) + \bar{G}(Z_1) \Gamma(Z_1, Z_2) \bar{G}(Z_2). \quad (3.5)$$

It can be shown, following Velicky,²⁰ that in CPA Γ can be written as

$$\Gamma = \sum_n |n\rangle \gamma \langle n| \quad (3.6)$$

and

$$\gamma(Z_1, Z_2) = \langle x/y \rangle t^A(Z_1) [\langle n | \bar{G}(Z_1) j \bar{G}(Z_2) | n \rangle \\ + \langle n | \bar{G}(Z_1) \gamma(Z_1, Z_2) \bar{G}(Z_2) | n \rangle \\ - \langle n | \bar{G}(Z_1) | n \rangle \gamma(Z_1, Z_2) \\ \times \langle n | \bar{G}(Z_2) | n \rangle] t^A(Z_2), \quad (3.7)$$

where we used $\langle t \rangle = 0$. Equation (3.7) is a 2×2 matrix equation which can be solved for γ . Velicky²⁰ has shown that γ vanishes for one-band model.

When band mixing is zero, the situation is analogous to that of two independent single-band CPA's. However, even then the γ 's do not vanish (see Appendix B).

IV. MODEL CALCULATION: NUMERICAL ILLUSTRATION

A. Model

In order to evaluate $\rho(E)$ we need to know $\bar{F}(Z)$. In the one-band model $\bar{F}(Z)$ is related to $F^0(Z)$ by a simple equation. The present case is more complicated, requiring an explicit integration over \vec{k} space to evaluate $F(E)$. For simplicity we assume

$$E_1(\vec{k}) + E_2(\vec{k}) = 0. \quad (4.1)$$

In the reduced-zone scheme this relation for semiconductors is at least qualitatively reasonable^{15,16} (Fig. 1). All quantities now can be expressed in terms of F_{11}^0 and F_{22}^0 which are again related to ρ_{11}^0 and ρ_{22}^0 through Eq. (2.13). Thus we need not know the explicit form for $E_1(k)$ or $E_2(k)$, and all we need to know are the densities of states $\rho_{11}^0(E)$ and $\rho_{22}^0(E)$. We assume the Hubbard model density

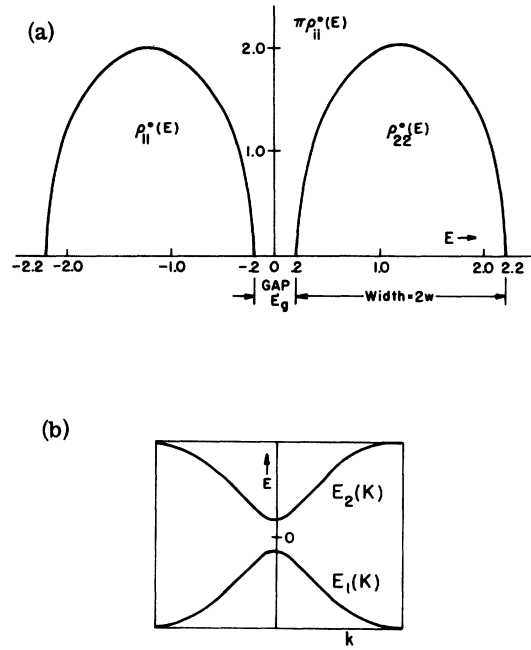


FIG. 1. Dispersion relation (b) (schematic) for the pure crystal $\epsilon^A = \epsilon^B = 0$, and the corresponding Hubbard model density of states (a).

of states for these bands;

$$\rho_{11}^0(E) = (2/w^2\pi)[w^2 - (E + \frac{1}{2}E_g + w)^2]^{1/2}, \quad (4.2) \\ \rho_{22}^0(E) = (2/w^2\pi)[w^2 - (E - \frac{1}{2}E_g - w)^2]^{1/2}.$$

Here $2w$ is the bandwidth and E_g the band gap. These have critical points at the band edges of the correct M_0 and M_3 types. We will show later that (4.2) gives an $\epsilon_2(\omega)$ dominated by one peak. The optical spectra of most of the semiconductors are known to be dominated by one major peak (Phillips¹⁴), and for a study of the systematics of $\epsilon_2(\omega)$ for alloys the above model density of states is good enough. A model calculation by Sak^{25,26} and three model densities of states (Hubbard model, simple cubic tight binding, and a density of states having all kinds of Van Hove singularities, composed of segments of parabolas) yielded the same gross features for ϵ_2 in three. After some algebra one obtains the following 2×2 matrix form (using a normalization of $w = 1$ henceforth) for Σ :

$$\Sigma = C - \frac{1}{4}\bar{F}' - \bar{F}^{-1}, \quad (4.3)$$

where

$$C = \begin{pmatrix} Z + \frac{1}{2}E_g + 1 & 0 \\ 0 & Z - \frac{1}{2}E_g - 1 \end{pmatrix}, \quad (4.4)$$

$$\bar{F}' = \begin{pmatrix} \bar{F}_{11} & -\bar{F}_{12} \\ -\bar{F}_{21} & \bar{F}_{22} \end{pmatrix}. \quad (4.5)$$

Equation (4.3) can be further simplified to a 2×2 matrix equation

$$4\bar{F}' = 16[C - \epsilon + (x-y)\delta] - [4(\epsilon - C + y\delta) + \bar{F}'] \\ \times \bar{F}[4(\epsilon - C - x\delta) + \bar{F}'] . \quad (4.6)$$

This equation involves only \bar{F} and \bar{F}' which do not have singularities.

B. Density of States: Parentage

We have shown in Figs. 4-6 the densities of states and parentage for several values of the parameters. For these examples we have used without any loss of generality,

$$\begin{aligned} \epsilon^A &= \frac{1}{2} \delta , \\ \epsilon^B &= -\frac{1}{2} \delta , \\ \epsilon &= \frac{1}{2}(x-y)\delta . \end{aligned} \quad (4.7)$$

The system of nonlinear equations (4.6) was solved by the Newton-Raphson²⁷ method. The quantities we are interested in are evaluated at energy $E + i0$. For the pure crystal we took $E_g = 0.4 (w = 1)$, which represents a typical value for semiconductors. In the one-band CPA there are two cases of major interest: split band and amalgamation. In the former, there are two subbands in the alloy density of states. In the latter there is a single band where the densities of states of the individual components have amalgamated. The term "band" used in this

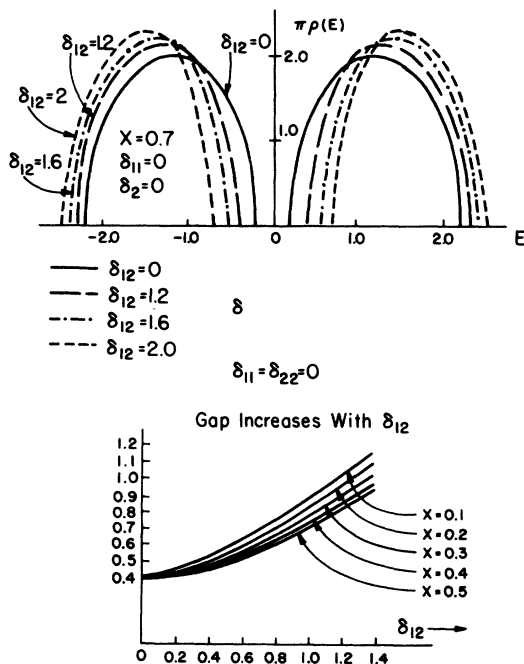


FIG. 2. Densities of states for various values of δ_{12} , where $\delta_{21} = \delta_{12}$ and $\delta_{11} = \delta_{22} = 0$. The gap is plotted for various values of δ_{12} and keeping $\delta_{11} = \delta_{22} = 0$.

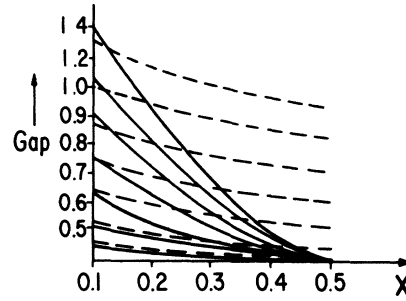


FIG. 3. Gaps for $\delta_{11} = \delta_{22} = 0$ for various values of x and δ_{12} are compared for the CPA and virtual crystal approximation (VCA). The dashed line is for the CPA and the solid lines correspond to the VCA. The various lines correspond to $\delta_{12} = 0.2, 0.4, 0.6, 0.8, 1.2,$ and 1.4 . The lines are plotted upwards as an increasing sequence of δ_{12} , the lowest lines corresponding to $\delta_{12} = 0.2$ and the highest ones to $\delta_{12} = 1.4$.

context implies well-defined regions in the density of states. In the two-band model, five mixed cases arise: conduction subbands and valence subbands can be separately amalgamated or split and furthermore they all can overlap forming a semimetal with no gap (Fig. 8).

Since the off-diagonal element δ_{12} plays a major role in our study, we consider its effect alone in Fig. 2. The gap increases almost quadratically with δ_{12} . The quadratic dependence is reminiscent of elementary perturbation theory where the level separation of two levels increases quadratically with the perturbation mixing them. The outer edges of the bands are affected relatively little compared to those near the gap. From a perturbation theory point of view, this can be attributed to the smaller energy denominator for the states near the band gap. In Fig. 3, we contrast some of the values obtained from CPA, with nonzero δ_{12} only, with those from the VCA as a function of composition (cf. Appendix A). The quadratic bowing of the energy gap with composition is typical in many semiconductors.¹⁸ The bowing of gap as a function of composition is obtained even in the VCA when δ_{12} is nonzero.

Next we show the density of states for varying δ_{12} in Figs. 4-8. These correspond to the strong scattering regime. The values of x , δ_{11} , and δ_{22} were kept fixed to illustrate the effects of band mixing δ_{12} which was varied systematically. The values of x , δ_{11} , and δ_{22} were so chosen that in the absence of band mixing ($\delta_{12} = 0$), the conduction band is in the amalgamation regime and the valence band is in the split band regime. This allows us to encompass all the trends in a brief series of numerical calculations. With increasing δ_{12} subbands start to split off, and eventually all bands split from each other. In all these cases the band gaps

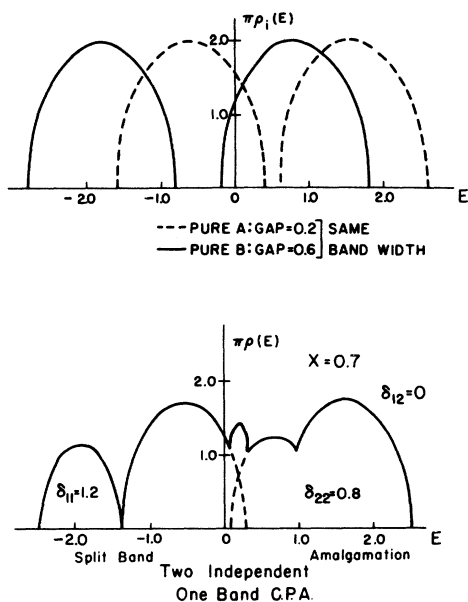


FIG. 4. In the upper half of the diagram we have plotted the densities of states of pure A and pure B material before alloying. The values δ_{11} and δ_{22} are 1.2 and 0.8, respectively, for an alloy of these. The lower part of the diagram corresponds to a CPA calculation with $x = 0.7$ and $\delta_{12} = 0$.

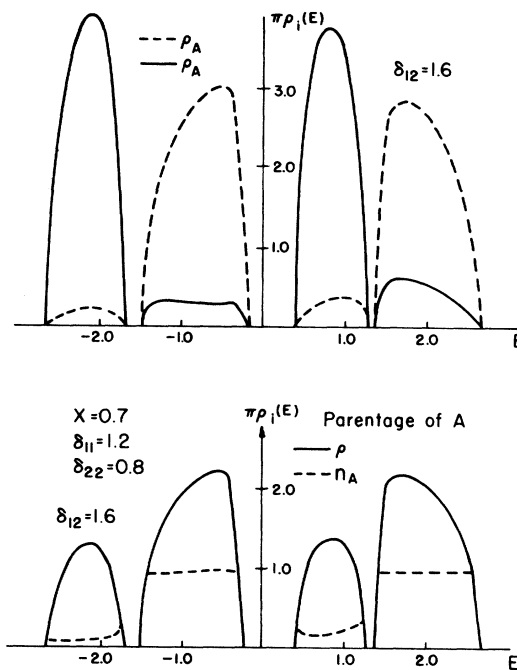


FIG. 6. Same as Fig. 5 except $\delta_{12} = 1.6$.

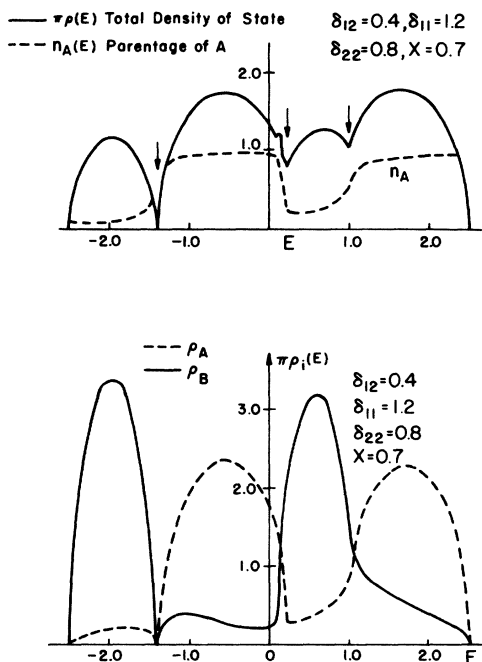


FIG. 5. x , δ_{11} , and δ_{22} are the same as in Fig. 4. Here $\delta_{12} = 0.4$. We have plotted the total density of states, the parentages η_A , ρ^A , and ρ^B . The pseudogaps are denoted by arrows.

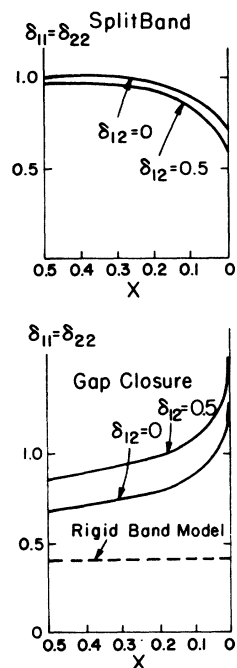


FIG. 7. Phase diagrams depicting various situations that can occur for $\delta_{12} = 0$ and $\delta_{12} = 0.5$ in the parameter space keeping $\delta_{11} = \delta_{22}$. In the upper diagram, the conduction subbands or the valence subbands split. In the lower diagram, the gap closes above the line indicated by gap closure. For higher values of δ_{12} the onset of gap closure requires a higher $\delta_{11} = \delta_{22}$ to overcome the additional band repulsion. The dashed lines correspond to the rigid-band model.

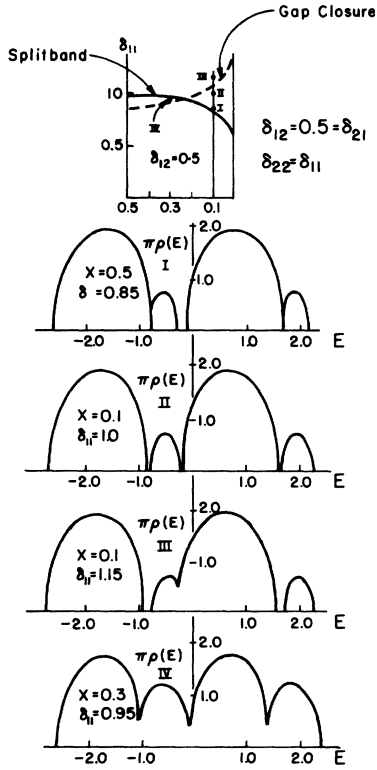


FIG. 8. Densities of states are plotted for four representative points in the phase diagrams for $\delta_{12}=0.5$.

are found to be smaller than those given by VCA (the values are given in the figures).

The band gaps in mixed crystals measured experimentally are usually found to have lower values than those predicted by VCA.¹⁸ In some other cases like in $\text{Ga}(\text{As}_x\text{P}_{1-x})$, the highest gaps have values higher than those for the VCA. Earlier, Stroud²⁸ has tried to explain these, combining the CPA and the golden rule. In our study, both cases arise naturally, depending on the values of the parameters. This is illustrated in Fig. 3. For the situation shown in Fig. 4, $x=0.7$, $\delta_{11}=1.2$, $\delta_{22}=0.8$, and $\delta_{12}=0$, we obtain a gap of 0.32 using the VCA as opposed to no gap in the CPA.

Again for the situation in Fig. 5, which is similar to that in Fig. 4 except here $\delta_{12}=0.8$, the VCA gives a gap of 0.36 as opposed to no gap in the CPA. If one increases δ_{12} further, as shown in Fig. 6, with $\delta_{12}=1.6$, one obtains a gap of 0.72 in the VCA again large compared to gap in the CPA. On the other hand, in the situation for Fig. 7, there is no gap closure in the VCA. The range of parameters which will give a zero gap in the CPA is shown in the same figure.

Using (4.3) it is easy to prove that around the pole for Σ ,

$$\bar{F}^{-1} \sim (\epsilon^B - C)(\epsilon + C)^{-1}(\epsilon^A - C). \quad (4.8)$$

Hence the poles occur at the energies given by $\det |C + \epsilon| = 0$. At these energies, $F \rightarrow 0$ as $\Sigma \rightarrow \infty$, and therefore $\rho \rightarrow 0$ and hence we have split band. The above equation has two roots. Only the poles in the first Riemann sheet are relevant. This provides the necessary condition, namely,

$$\rho(E + i0) \geq 0. \quad (4.9)$$

Equation (4.9) implies for $\delta_{12}=0$ and $\delta_{11}=\delta_{22}$, that

$$xy\delta_{ii}^2 \geq \frac{1}{4} \quad (i=1, 2), \quad (4.10)$$

and when δ is purely off diagonal the necessary condition is

$$xy\delta_{12}^2 \geq \frac{1}{4}. \quad (4.11)$$

In Fig. 8, sequences I–III show how the subbands split, eventually closing some gaps and opening others going through a semimetallic phase. The opening and closing of gaps as a function of composition are well known in alloys like $\text{Pb}_{1-x}\text{Sn}_x\text{Te}$ and $\text{Hg}_{1-x}\text{Cd}_x\text{Te}$.¹⁸

The parentages of the states are illustrated in Figs. 5 and 6; it is obvious that we can unmistakably identify which band arises from which material. The vestiges of conduction and valence band structures are also obvious. The latter result reinforces the hypothesis in the Mott-CFO^{4,24} model about the retention of parentage by the localized states in the gap. In Fig. 6 we see that even in the presence of large band mixing, which causes bands to split, ρ^A and ρ^B individually show the valence band and the conduction band parentages.

Let us define the quantity n_i as follows:

$$n_i(E) = \rho^i(E)/\rho(E) \quad (i=A \text{ or } B). \quad (4.12)$$

According to Economou *et al.*¹⁰ the pseudogaps occur near where there is a sharp discontinuity in n_i , or where n_i is large compared to the concentration of the i th component itself. Such possible pseudogaps are indicated by arrows in the diagrams. ρ^A denotes the density of states at a site occupied by A, and when ρ^A is large compared to ρ^B , we can say, semiclassically, that the states corresponding to these energies are formed mainly by channels of A with B fluctuating in the path. A sudden drop in n_A would imply that these channels are blocked by fluctuations of high local B concentration.

C. dc Conductivity and $\epsilon_2(\omega)$

In order to evaluate the transport properties explicitly, we need to know the expectation value of the current (or equivalently dipole) operators. The interband matrix element of the dipole moment is very often assumed constant over the Brillouin zone, with some justification.²⁹ Accordingly we

shall take it as a constant. Time reversal requires that $\langle \vec{k}i | j | -\vec{k}'i' \rangle = -\langle \vec{k}i | j | \vec{k}i \rangle^*$; so we can write,

$$j_\mu(k) = e \begin{pmatrix} \frac{\partial E_1(\vec{k})}{\partial k_\mu} & ai \\ -ai & \frac{\partial E_2(\vec{k})}{\partial k_\mu} \end{pmatrix}, \quad (4.13)$$

where a is a real constant and e the electronic charge.

In order to obtain σ and $\epsilon_2(\omega)$, it turns out that we do not have to know $\partial E_1(\vec{k})/\partial \vec{k}$ or $\partial E_2(\vec{k})/\partial \vec{k}$ explicitly; all we need to know are quantities like

$$\sum_{\vec{k}} \left(\frac{\partial E_i(\vec{k})}{\partial \vec{k}} \right)^2 \delta(E - E_i(k)).$$

We assume, following Velicky,²⁰

$$\begin{aligned} P_{11}(\xi) &= \sum_{\vec{k}} \left(\frac{\partial E_1(\vec{k})}{\partial \vec{k}} \right)^2 \delta(\xi - E_1(\vec{k})) \\ &= b \left[1 - (\xi + 1 + \frac{1}{2} E_g)^2 \right]^{3/2}, \\ P_{22}(\xi) &= \sum_{\vec{k}} \left(\frac{\partial E_2(\vec{k})}{\partial \vec{k}} \right)^2 \delta(\xi - E_2(\vec{k})) \\ &= b \left[1 - (\xi - 1 - \frac{1}{2} E_g)^2 \right]^{3/2}, \end{aligned} \quad (4.14)$$

where b is a real constant. We have estimated using the f -sum rule that $a^2/b \sim \frac{1}{25}$. When we compare the numerical illustrations given by Velicky²⁰ using an approximation like (4.14) for a single band with the calculations of Levine *et al.*²¹ using a simple tight-binding model for $E(\vec{k})$, and corresponding exact forms for P_{11} and P_{22} , we find that the gross features remain the same in both cases, justifying our use of (4.14). The reason being that the M_1 and M_2 Van Hove singularities missing from the Hubbard density of states, tend to smooth out in an alloy.

Numerical examples for the dc conductivity $\sigma(E)$ as a function of the energy E are presented in Figs. 9(a) and 9(b). The contribution to $\sigma(E)$ from the part which involves $(j_{12})^2$ is not plotted separately because this is small compared to the intraband part, as expected. (Similarly, the vertex correction turns out to be very small in this case and is not shown in the figures.)

$\sigma(E)$ shows a tailing near the band edges and is much smaller in the minority subband compared to that in the majority subband. In other words the states with lower $\sigma(E)$ correspond to lower mobility.¹ On the other hand, from the density-of-states considerations alone this is not obvious. At a finite temperature, when there is a minority subband adjacent to the band gap we expect that dc measurements will indicate through the form $\sigma \propto e^{-E_g/KT}$ a larger band gap than that estimated from density-of-states plot.

However these states in the minority subband are

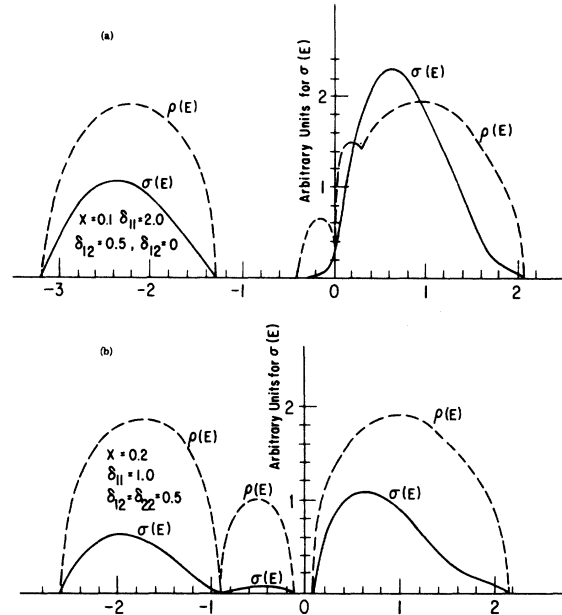


FIG. 9. Density of states and $\sigma(E)$ are plotted. A significant drop of $\sigma(E)$ occurs near the energy where the bands split (possible pseudogap, see Fig. 5).

perfectly accessible to optical transition and optical measurements will indicate a gap identical to that in the density of states, provided that the dipole matrix element does not change. This is clear from the plot of $\epsilon_2(\omega)$ given in Fig. 10. When $\delta_{22}=0$, $\delta_{11}=0$, and $\delta_{12}=0$, the analytic behavior for $\omega^2 \epsilon_2(\omega)$ in the alloy is found to be linear in $\omega - E_g$, whereas in the pure crystal it goes as $\omega - E_g$. (See discussion in Appendix C.) For the reason of computational time and expense we did not plot $\epsilon_2(\omega)$ for large ω where $1/\omega^2$ will dominate the structure. We do not find any tailing in $\omega^2 \epsilon_2$ as in some early experiments on amorphous materials by Tauc.³⁰ Recent experiments by Wood and Tauc³¹ on three bulk semiconductor glasses report a weak absorption tailing near the absorption edge. These tailing effects are due to a transition from localized states to itinerant states and beyond the scope of a CPA calculation. In most of the semiconductors (e.g., selenium and silicon) one observes a sizable decrease in the peak of $\epsilon_2(\omega)$ in going from crystalline to amorphous form.^{1,32} We have plotted $\epsilon_2(\omega)$ for a perfect crystal with the gap adjusted to that of the alloy in Fig. 10. In Fig. 11, we see that $\omega^2 \epsilon_2$ goes as $(\omega - E_g)^2$ near the gap for $\delta_{11}=1.0$, $\delta_{22}=0.5$, and $x=0.2$. This kind of dependence is seen in some amorphous materials. [We refer to the book by Mott¹ for more details about the various forms of the analytic behavior of $\omega^2 \epsilon_2(\omega)$.] There is a sizable drop in going from the crystal to the alloy. We should mention that Krammer *et*

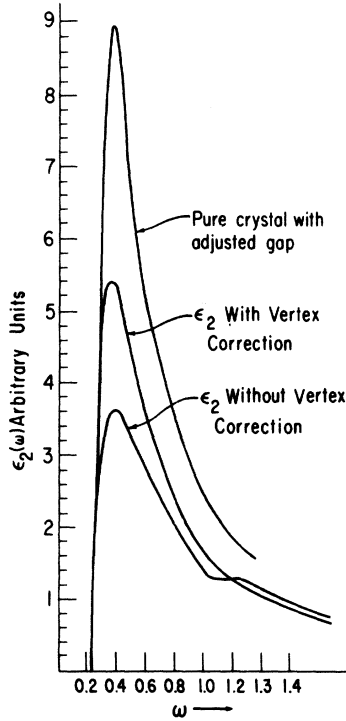


FIG. 10. $\epsilon_2(\omega)$ is plotted against ω for an alloy: $x = 0.2$, $\delta_{11} = 1.0$, $\delta_{12} = \delta_{22} = 0.5$. The vertex correction enhances the peak. For comparison we have plotted $\epsilon_2(\omega)$ for a pure crystal with its gap adjusted to that of the alloy given by the CPA.

al.,³³ using a convoluted density of states and relaxing the \vec{k} -conservation selection rule for interband transitions, obtained a remarkable agreement with the experimental curve. $\epsilon_2(\omega)$ for the convoluted density of states with the relaxation of the \vec{k} -conservation rule is given by

$$\epsilon_2(\omega) \propto \frac{4\pi^2}{\omega^2} \int \rho_{\text{val}}(E) \rho_{\text{CON}}(E + \omega) dE. \quad (4.15)$$

For the CPA we can extract a factor $M(E, \omega)$ such that

$$\epsilon_2(\omega) \propto \frac{4\pi^2 \alpha^2}{\omega^2} \int \rho_{11}(E) \rho_{22}(E + \omega) M(E, \omega) dE. \quad (4.16)$$

In Appendix C, for a simple case where δ_{22} and δ_{12} are zero and δ_{11} small, we obtain analytically

$$M(E, \omega) \propto \frac{xy\delta^2}{[2E + \omega - \text{Re}\Sigma_{11}(E)]^2 + [\text{Im}\Sigma_{11}(E)]^2} \quad (4.17)$$

and $\omega^2\epsilon_2(\omega)$ has a linear edge. However, in amorphous selenium Davis¹ observed the linear dependence, $\omega^2\epsilon_2(\omega)$ vs $\omega - E_g$. The similarity of our $\epsilon_2(\omega)$ spectrum for the alloy to that of selenium is rather remarkable.

The effect of the vertex correction can be seen to increase the peak in $\epsilon_2(\omega)$. This is obviously the result of taking into account the effect of correlations of the electron and hole. The completely correlated case corresponds to that of the pure crystal with a larger hump. The behavior at the edge is similar to that where γ is neglected (Fig. 11).

V. CONCLUSION

It is clear that CPA illuminates qualitatively many features of disordered media: the size of the gap, the edges of the optical spectrum, and the question of parentage. The formalism revealed an important analytical result that the vertex correction is not zero as we go beyond one band, even when there is no band mixing. Eggarter *et al.*³⁴ proved exactly that the average of a single Green's function cannot give the transport properties and a considerable amount of information is simply lost in averaging the single Green's function. In this respect, the generalization of the CPA for transport properties is quite good: It obtains an average of a product of two Green's function. The vertex correction corresponds to the additional correction over the simple averaged Green's function, i. e., $\langle G_j G \rangle = \bar{G} j \bar{G} + \bar{G} \Gamma G$. Nevertheless, the CPA provides only a single-site approximation for Γ . In our model calculation it has turned out that Γ is given solely as a functional of $\bar{G}(Z)$:

$$\Gamma(Z_1, Z_2) = \Gamma(\bar{G}(Z_1), \bar{G}(Z_2)).$$

Thus the calculation of Γ using the CPA is incomplete. It would therefore be interesting to

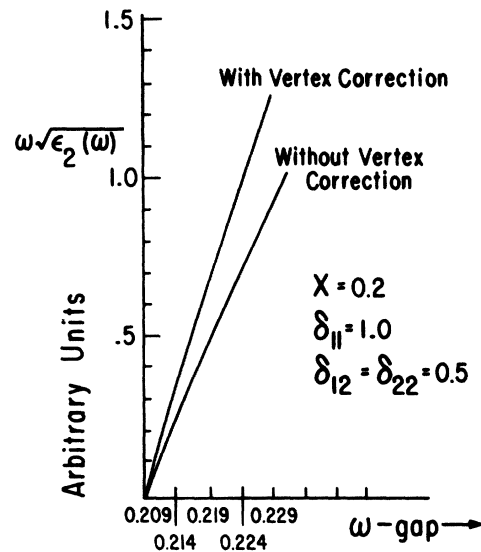


FIG. 11. $\omega^2\epsilon_2(\omega)$ is shown to behave quadratically with $\omega - E_g$ for $\epsilon_2(\omega)$ with and without vertex correction, near threshold.

study the behavior of $\langle G \otimes G \rangle$ itself and to be able to obtain a self-consistent approximation for it using a method like the Cohen-Freed³⁵ extension of the CPA to go beyond the single-site approximation.

ACKNOWLEDGMENTS

It is a great pleasure to thank my thesis sponsor, Professor M. H. Cohen, for suggesting this problem and for his constant guidance and encouragement. I would also like to thank Professor H. Fritzsche for many useful discussions. Finally I would like to thank the members of solid state theory group at The University of Chicago for much help.

APPENDIX A: GAP IN THE VIRTUAL CRYSTAL

The Hamiltonian for the pure A and B crystals can be written in the same fashion as (2.1):

$$H^{A,B} = \sum_n |n\rangle \epsilon^{A,B} \langle n| + \sum_m |m\rangle t_{mn} \langle n|, \quad (\text{A1})$$

$$H_{vc} = xH^A + yH^B. \quad (\text{A2})$$

To obtain the gap E_g in the relevant crystals, we have to diagonalize H_{vc} . In the model calculations we have taken $E_1(\vec{k}) + E_2(\vec{k}) = 0$. This gives the gap

at $\vec{k} = 0$ in the VCA, \bar{E}_g :

$$\bar{E}_g = [(\epsilon_{11} - \epsilon_{22} - E_g)^2 + 4\epsilon_{12}\epsilon_{21}]^{1/2}. \quad (\text{A3})$$

If $\epsilon_{11} = \epsilon_{22} = 0$, then

$$\bar{E}_g = [E_g^2 + 4\epsilon_{12}\epsilon_{21}]^{1/2} \geq E_g. \quad (\text{A4})$$

Note that if $\epsilon_{12} = 0$, i.e., when there is no band mixing, the gap varies linearly with x . Calculations by Van Vechten *et al.*¹⁸ yield a linear variation of gap with x in the VCA. However the experimental gap they quote varies quadratically with x .¹⁸ This clearly demonstrates that interband scatterings are very important for $\delta_{12} \neq 0$, when we indeed get the characteristic bowing of the gap even in the VCA.

APPENDIX B: REMARKS ON VERTEX CORRECTIONS

When $\delta_{12} = 0$ the situation is analogous to two independent one-band CPA's, yet γ does not vanish. Let us demonstrate this using (3.5) and remembering that when $\delta_{12} = 0$, t , \bar{F} , Σ , and G reduce to diagonal form in the band indices. Then invoking the usual argument about oddness of $\partial E / \partial k$ and evenness of $G(Z, \vec{k})$ in \vec{k} space, we get from (3.7)

$$\gamma_{11}(Z_1, Z_2) = \gamma_{22}(Z_1, Z_2) = 0,$$

but

$$\gamma_{12}(Z_1, Z_2) = \frac{x}{y} \frac{t_{11}^A(Z_1) t_{22}^A(Z_2) (ia) \Omega_{11,22}(Z_1, Z_2)}{1 + (x/y) t_{11}^A(Z_1) [F_{11}(Z_1) F_{22}(Z_2) - \Omega_{11,22}(Z_1, Z_2)]},$$

where

$$\Omega_{ij,kl} = \frac{1}{N} \sum_{\vec{k}} \bar{G}_{ij}(Z_1, \vec{k}) \bar{G}_{kl}(Z_2, \vec{k}).$$

APPENDIX C: ANALYTICAL PROPERTIES OF ϵ_2

In a simple case where $\delta_{11} \neq 0$ but $\delta_{12} = \delta_{21} = \delta_{22} = 0$, it can be shown that since $t_{22} = 0$ and $t_{12} = 0$, $\gamma \neq 0$ for this case. Writing $\Sigma_{12} = \Sigma_{21} = \Sigma_{22} = 0$ in this case, we have from (3.3)

$$\omega^2 \epsilon_2(\omega) \propto \int dE \frac{2 \text{Im} F_{22}^0(E + \omega) \text{Im} \Sigma_{11}(E^*)}{[2E + \omega - \text{Re} \Sigma(E^*)]^2 + [\text{Im} \Sigma(E^*)]^2}. \quad (\text{C1})$$

Now in the weak scattering limit when $\delta_{11} \rightarrow 0$ we obtain (2.15):

$$\omega^2 \epsilon_2(\omega) \propto \int dE \frac{xy \delta_{11}^2 \rho_{22}^0(E + \omega) \rho_{11}^0(E - \epsilon_{11})}{[2E + \omega - \text{Re} \Sigma_{11}(E^*)]^2 + [xy \delta_{11}^2 \pi \rho_{11}^0(E - \epsilon)]^2}.$$

The center of gravity of ρ_{11}^0 has been shifted by ϵ_{11} , whereas the ρ_{22}^0 was unaffected. Hence the effective gap is now $E_g - \epsilon_{11}$. Let

$$\Delta\omega = \omega - (E_g - \epsilon), \quad Z = E + \omega - \frac{1}{2} E_g; \quad (\text{C2})$$

then

$$\omega^2 \epsilon_2(\omega) \propto \int_0^{\Delta\omega} dE \frac{[Z(\Delta\omega - Z)]^{1/2} (\pi xy \delta^2)}{(2Z - \Delta\omega)^2 + 2(\pi xy \delta^2)^2 (\Delta\omega - Z)}.$$

When $\Delta\omega \rightarrow 0$ but $\delta \gg \Delta\omega$, we get

$$\omega^2 \epsilon_2(\omega) \propto \Delta\omega = \omega - E_g + \epsilon.$$

When $\Delta\omega \rightarrow 0$ but $\delta \ll \Delta\omega$, we get

$$\omega^2 \epsilon_2(\omega) \propto (\omega - E_g)^{1/2} \quad (\text{crystalline case}).$$

For the pure crystal when $\epsilon^A = \epsilon^B = 0$, Eq. (3.3)

gives

$$\epsilon_2^0(\omega) = (2\pi^2 e^2 / m^2 \omega^2) |p_{12}|^2 \rho_{22}^0(\frac{1}{2}\omega)$$

or

$$\omega^2 \epsilon_2^0 \propto (\omega - E_g)^{1/2} .$$

*Submitted in partial satisfaction of the requirements for the Ph.D degree at The University of Chicago.

†Work supported in part by the ARO(D) and benefited from support of Materials Science at The University of Chicago by ARPA and the NSF.

‡Present address: Xerox Palo Alto Research Center, Palo Alto, Calif. 94304.

¹N. F. Mott and E. A. Davis, *Electronic Processes in Non-Crystalline Materials* (Clarendon, Oxford, England 1971).

²M. H. Cohen, in *Proceedings of the Tenth International Conference on Physics of Semiconductors*, Cambridge, Mass. (1970), edited by S. P. Keller, I. C. Hansel, and F. Stern (U.S. AEC Division of Technical Information, Washington, D.C., 1970).

³Proceedings of Fourth International Conference on Amorphous and Liquid Semiconductors, Ann Arbor, Mich., 1971 (unpublished).

⁴M. H. Cohen, H. Fritzsche, and S. R. Ovshinsky, *Phys. Rev. Lett.* **22**, 1065 (1969).

⁵P. Soven, *Phys. Rev.* **156**, 809 (1967); *Phys. Rev.* **178**, 1136 (1969).

⁶B. Velicky, S. Kirkpatrick, and H. Ehrenreich, *Phys. Rev.* **175**, 747 (1968), henceforth to be called VKE.

⁷D. W. Taylor, *Phys. Rev.* **156**, 1017 (1967).

⁸E. Siggia and L. Schwartz, *J. Non-Cryst. Solids* **8-10**, 140 (1972).

⁹Y. Onodera and J. Toyozawa, *J. Phys. Soc. Jap.* **24**, 341 (1968).

¹⁰E. N. Economou, S. Kirkpatrick, M. H. Cohen, and T. P. Eggarter, *Phys. Rev. Lett.* **25**, 1520 (1970).

¹¹S. Kirkpatrick, B. Velicky, and H. Ehrenreich, *Phys. Rev. B* **1**, 3250 (1970).

¹²K. Levin and H. Ehrenreich, *Phys. Rev. B* **3**, 4172 (1971).

¹³D. Stroud and H. Ehrenreich, *Phys. Rev. B* **2**, 3197 (1970).

¹⁴J. C. Phillips, *Covalent Bonding in Crystals, Molecules and Polymers* (University of Chicago Press, Chicago, 1970).

¹⁵D. R. Penn, *Phys. Rev.* **128**, 2093 (1962).

¹⁶V. Heine and R. O. Jones, *J. Phys. C* **2**, 719 (1969).

¹⁷P. N. Sen and M. H. Cohen, *J. Non-Cryst. Solids* **8-10**, 147 (1972).

¹⁸J. A. Van Vechten, O. Beroto, and J. C. Woolley, *Phys. Rev. Lett.* **29**, 1400 (1972); G. A. Saunders, *Contemp. Phys.* **14**, 149 (1973).

¹⁹R. Kubo, *J. Phys. Soc. Jap.* **12**, 570 (1957).

²⁰B. Velicky, *Phys. Rev.* **184**, 614 (1969).

²¹K. Levine, B. Velicky, and H. Ehrenreich, *Phys. Rev. B* **2**, 1771 (1970).

²²J. M. Lifshitz, *Usp. Fiz. Nauk* **83**, 617 (1964) [*Sov. Phys.-Usp.* **7**, 549 (1965)].

²³G. F. Koster and J. C. Slater, *Phys. Rev.* **96**, 1208 (1954).

²⁴G. Srinivasan and Morrel H. Cohen, *J. Non-Cryst. Solids* **3**, 393 (1970).

²⁵J. Sak (unpublished).

²⁶P. Lloyd, *J. Phys. C* **2**, 1717 (1969).

²⁷B. Carnahan, H. A. Luther, and J. O. Wilkes, *Applied Numerical Methods* (Wiley, New York, 1969).

²⁸D. Stroud, *Phys. Rev. B* **5**, 3366 (1972).

²⁹D. Brust, *Phys. Rev.* **5**, A1337 (1964).

³⁰J. Tauc, in *Optical Properties of Solids*, edited by S. Nudelman and S. Mitra (Plenum, New York, 1969).

³¹D. L. Wood and J. Tauc, *Phys. Rev. B* **5**, 3144 (1972).

³²J. Stuke, *J. Non-Cryst. Solids* **4**, 1 (1970).

³³B. Kramer, K. Maschke, P. Thomas, and J. Treusch, *Phys. Rev. Lett.* **25**, 1020 (1970).

³⁴T. P. Eggarter, M. H. Cohen, and E. N. Economou, *Solid State Commun.* **12**, 1013 (1973).

³⁵K. Freed and M. H. Cohen, *Phys. Rev. B* **3**, 3400 (1971).